ANNALS OF PHYSICS 177, 330–358 (1987)

Periodic Trajectories for a Two-Dimensional Nonintegrable Hamiltonian*

M. BARANGER

Center for Theoretical Physics, Laboratory for Nuclear Science, and Department of Physics, Massachusetts Institute of Technology, Cambridge, Massachusetts 02139

AND

K. T. R. DAVIES

Physics Division, Oak Ridge National Laboratory, Oak Ridge, Tennessee 37831-6373, and Center for Theoretical Physics, Laboratory for Nuclear Science, Massachusetts Institute of Technology, Cambridge, Massachusetts 02139

Received April 17, 1987

A numerical study is made of the classical periodic trajectories for the two-dimensional, nonintegrable Hamiltonian

$$H = \tfrac{1}{2}(p_x^2 + p_y^2) + (y - \tfrac{1}{2}x^2)^2 + 0.05\, x^2.$$

In addition to x–y pictures of the trajectories, E–τ (energy–period) plots of the periodic families are presented. Efforts have been made to include all trajectories with short periods and all simple branchings of these trajectories. The monodromy matrix has been calculated in all cases, and from it the stability properties are derived. The topology of the E–τ plot has been explored, with the following results. One family may have several stable regions. The plot is not completely connected; there are islands. The plot is not a tree; there are cycles. There are isochronous branchings, period-doublings, and period-multiplyings of higher orders, and examples of each of these are presented. There is often more than one branch issuing from a branch point. Some general empirical rules are inferred. In particular, the existence of isochronous branchings is seen to be a consequence of the symmetry of the Hamiltonian. All these results agree with the general classification of possible branchings derived in Ref. [10]. (M. A. M. de Aguiar, C. P. Malta, M. Baranger, and K. T. R. Davies, in preparation). Finally, some nonperiodic trajectories are calculated to illustrate the fact that stable periodic trajectories lie in "regular" regions of phase space, while unstable ones lie in "chaotic" regions.

I. INTRODUCTION

This paper presents extensive numerical data concerning the periodic classical trajectories of a particle moving in a nonintegrable, two-dimensional potential. This field of mechanics is very badly known although it is highly relevant to many domains of research, both classical and quantal, some of which we shall mention later. For now, we just repeat the famous quote from Poincaré [1]: "What renders these periodic solutions so precious to us is that they are, so to speak, the only breach through which we might try to penetrate into a stronghold hitherto reputed unassailable."

* The submitted manuscript has been authored by a contractor of the U.S. Government under contract DE-AC05-84OR21400. The U.S. Governement's right to retain a nonexclusive royalty-free license in and to the copyright covering this paper, for governmental purposes, is acknowledged.

0003-4916/87 $7.50

These results were made possible by the development of computational methods especially adapted to the search for periodic trajectories and much faster than the usual procedure involving Poincaré sections. The details will appear elsewhere [2]. An important aspect of these methods is that, unlike that which uses Poincaré sections, they work as well for unstable as for stable periodic trajectories. It has been recognized [4] that unstable periodic trajectories can play an important role in the quantization problem.

In fact, our motivation for studying this problem came mostly from a desire to understand quantization. Why should one quantize classical trajectories rather than simply start from the Schrödinger equation? Because it is frequently true, in many-body problems, that one can obtain, relatively easily, approximate solutions of the Schrödinger equation in the form of time-dependent wave packets which follow classical-like trajectories. The time-dependent Hartree–Fock and other time-dependent mean-field approximations [5] are of this type. And why should one want to do this quantization using periodic classical trajectories? Because, as Poincaré knew [1], the periodic trajectories, by themselves, already contain all possible information about the dynamics, and they are easier to work with, since any desired time integral needs to be done only over one period, rather than from $-\infty$ to $+\infty$; one can always refine the answers by looking at longer periods. Much work has been done toward using periodic trajectories in quantization [4, 6], but some aspects of the problem still remain unsolved.

Some of the results presented here have previously appeared in Ref. [7]. The structure of the remainder of this paper is as follows. In Section II we discuss some general features of the monodromy matrix and its associated branching behavior, we give the two-dimensional Hamiltonian used in our work, and we define the symbols and notations appearing in the figures. The detailed numerical results for the most important periodic families are presented in Section III, together with some general empirical rules. In Section IV we illustrate briefly how the behavior of the nonperiodic trajectories is related to the stability of nearby periodic families.

II. General Definitions

A periodic trajectory has an energy E and a period τ. It is well known [8] that periodic trajectories occur in one-parameter families, each of which defines a continuous curve in the E–τ plane. Hence, most of our data are presented in the form of E–τ plots. This set of lines is characteristic of the Hamiltonian H being studied; just as in quantum mechanics the set of energy levels is characteristic of H. It is important to study the geometry and the topology of the E–τ plot.

Another very useful characteristic of each periodic trajectory is its monodromy matrix M [9], whose eigenvalues are the Floquet–Lyapunov multipliers. This is the matrix which describes, after one period, the change in position and velocity due to a small arbitrary change in initial conditions. For two space dimensions, M is a 4×4 matrix. Two eigenvalues of M are always unity [9]. The other two have unit product and can be either complex conjugates (of the form $e^{i\alpha}$, $e^{-i\alpha}$) or real (of the

form $\pm e^{\beta}, \pm e^{-\beta}$). In the former case, the trajectory is stable and the trace of M lies between 0 and 4. In the latter, the trajectory is unstable and Tr M lies outside the interval (0, 4).

The topology of the E–τ plot is determined by its branchings. At an isochronous branching (where the period does not change) there is a confluence of two distinct families of periodic trajectories; therefore, M has four unit eigenvalues and Tr $M=4$. At a period-doubling branching, two eigenvalues must be -1; hence Tr $M=0$. There are also period-triplings (Tr $M=1$), period-quadruplings (Tr $M=2$), and so on. In the next section we present a number of examples of both isochronous and period-multiplying branchings. Obviously, the E–τ plot at large τ becomes dense and complicated. But it is not "everywhere dense," unlike a plot of the periodic trajectories in coordinate or phase space; the families are discrete and the most important families, as well as the lowest density of E–τ curves, are found at small τ.

Let us comment very briefly on the numerical solutions. For a two-dimensional potential, $V(x, y)$, and a particle of unit mass, the classical equations of motion are

$$\ddot{x}+\frac{\partial V}{\partial x}(x, y)=0 \tag{1a}$$

$$\ddot{y}+\frac{\partial V}{\partial y}(x, y)=0, \tag{1b}$$

where the dot indicates a time derivative. The simplest discretization of these equations on a time mesh is

$$\frac{x_{n+1}-2x_n+x_{n-1}}{\varepsilon^2}+\frac{\partial V}{\partial x}(x_n, y_n)=0 \tag{2a}$$

$$\frac{y_{n+1}-2y_n+y_{n-1}}{\varepsilon^2}+\frac{\partial V}{\partial y}(x_n, y_n)=0, \qquad n=0, 1, 2, ..., N-1, \tag{2b}$$

where N is the total number of time steps. For a periodic solution, we impose the conditions

$$\begin{aligned}(x_N, y_N)&=(x_0, y_0)\\ (x_{N+1}, y_{N+1})&=(x_1, y_1),\end{aligned} \tag{3}$$

and

$$\tau=N\varepsilon \tag{4}$$

gives the period of the motion. In Ref. [2] we present a very fast method for solving these equations utilizing the properties of the monodromy matrix [9].

All of the calculations of this paper were done by applying this method to the following potential (code name NELSON)

$$V(x, y)=\left(y-\frac{x^2}{2}\right)^2+\mu\frac{x^2}{2} \qquad (\mu=0.1). \tag{5}$$

The NELSON potential consists of a deep valley in the shape of a parabola, surrounded by high mountains. See the contour plot in Fig. 1. Note the symmetry

with respect to the y-axis. Interest in NELSON was motivated by nuclear physics, where the deep valley could represent a collective degree of freedom which, however, remains coupled to other types of excitation. Similar studies of periodic trajectories have been performed for three other potentials (code names MARTA, MARCO, and DELFI) and will be published separately (e.g., Ref. [10]). Others are under investigation. Actually, we do not expect the topological phenomena we are reporting in this paper to depend essentially on the Hamiltonian used, except for effects associated with the $x \to -x$ symmetry in Eq. (5). It turns out that symmetry has an important influence on the types of branchings occurring; this is discussed in detail in Ref. [10]. Unfortunately, the anisotropic Kepler Hamiltonian, for which Gutzwiller [11] obtained a famous exact solution, is too special to be of interest in our context: because of the very simple scaling property, the E–τ plot for this problem has no interesting structure and shows no branchings. The same is true of the various "billiards" [12] problems.

Time-reversal invariance dictates that there be two kinds of periodic trajectories, which are traditionally known as *librations* (the trajectory is its own time-reverse; hence the particle follows the same path in both directions, with turning points at the ends) and *rotations* (the particle follows a closed path in one direction only; the direction is opposite for the time-reversed trajectory). On our E–τ plots, we label the rotations by a Greek ρ; all families not so marked are librations. We also indicate the range of Tr M by using heavy lines or the symbol s for stable trajectories, and thin lines or the symbol u for unstable ones. In general, stable trajectories lie in regular regions of phase space and unstable ones lie in chaotic regions

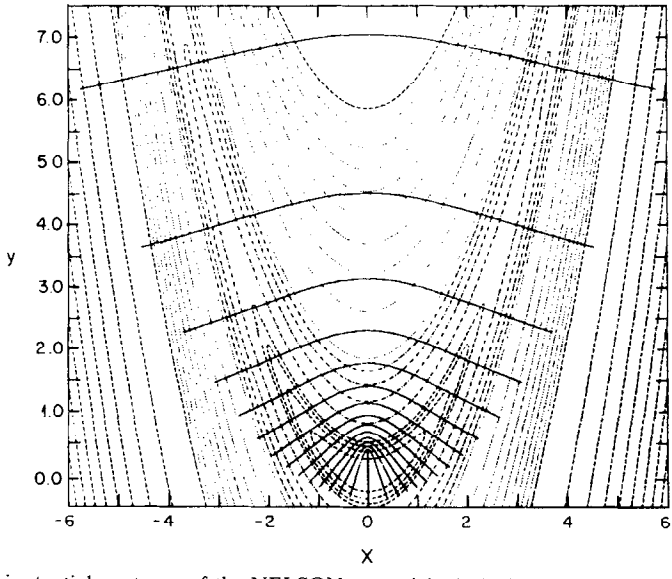

FIG. 1. Equipotential contours of the NELSON potential (dashed and dotted lines), with members of the B, or "boomerang," family of symmetric librations (full lines), which begins at low energy as a period-doubling from the vertical family. The boomerang curves become flatter as the energy increases and they extend to infinite energy.

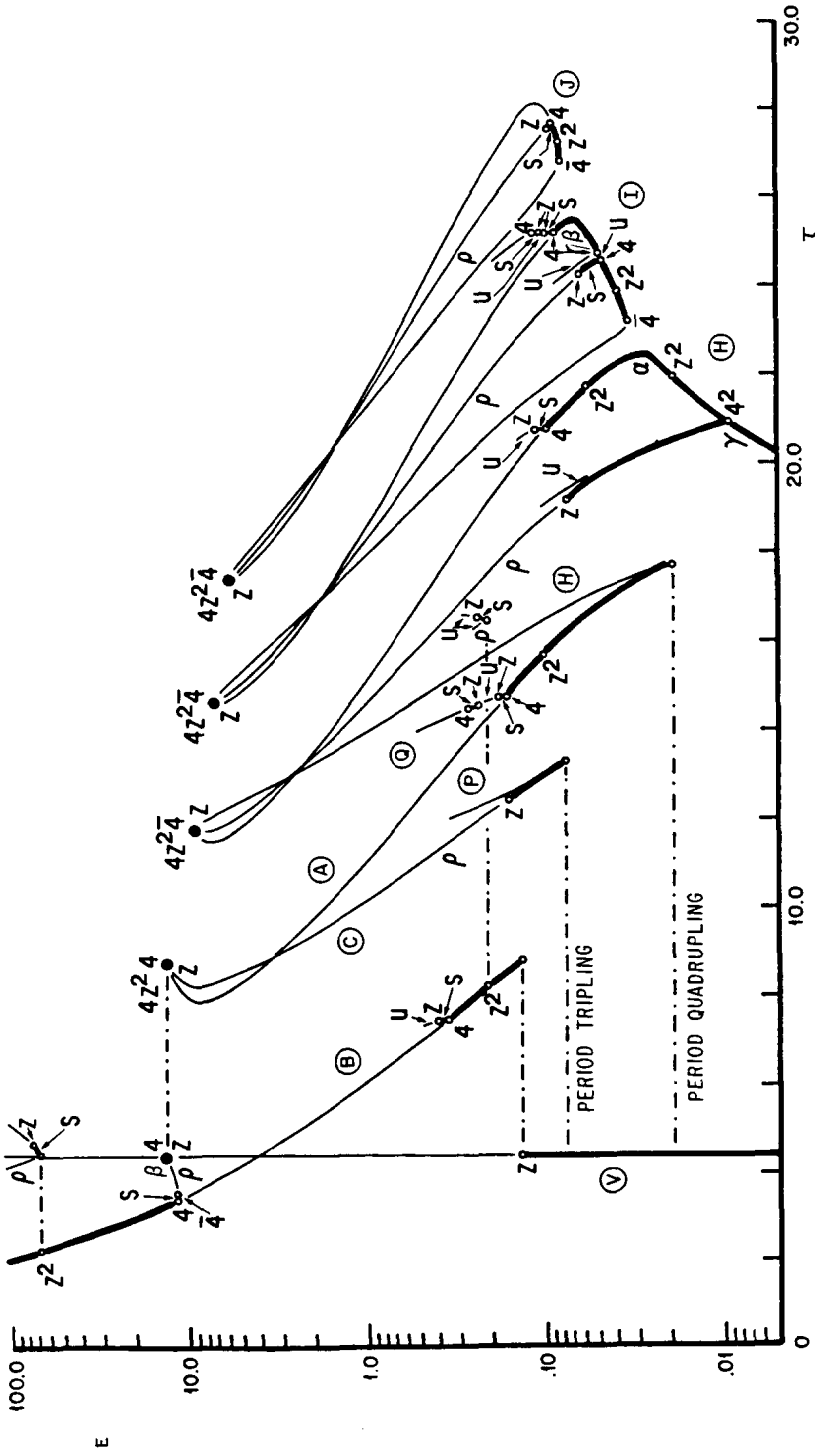

FIG. 2. E–τ plot of the main symmetric families, showing also the beginnings of asymmetric branchings. The circled capital letters are the family names. The full circle at the top of each of the A, H, I, and J families contains a small concentrated region of stability, examples of which are shown in Fig. 4 and the inset to Fig. 3. The symbols α, β, and γ are defined in Section III; the remaining symbols are defined in Section II.

[13, 14]; for more about this, see Section IV. The limiting values of Tr M, 4 and Z (for "zero"), are also marked on the plots; a double solution to Tr $M = 0$, i.e., a place in the plot Tr M vs τ (or E) where Tr M goes through zero with a horizontal tangent, is indicated by Z^2, and similarly for 4^2. In the next section we present examples showing that such a tangency always gives rise to several distinct branches. The notation $\bar{4}$ ("horizontal" 4) indicates that Tr M is equal to 4 at a horizontal tangent in the E–τ plane, i.e., $dE/d\tau = 0$. Also, on the E–τ plots, a small filled circle indicates a tiny region of stability which may also include an even smaller region of instability. For example, a filled circle with $4\,Z\,Z\,\bar{4}$ means that Tr M first goes through 4 and then goes to zero (stable region), after which it briefly becomes negative (unstable region), goes through zero again, and then passes through a horizontal 4 (stable region).

Since our potential has the $x \to -x$ symmetry, we usually distinguish between symmetric and asymmetric families. The frequent occurrence of Z^2 and 4^2 branchings seems to be a property of the symmetric families; for more about this, see Ref. [10].

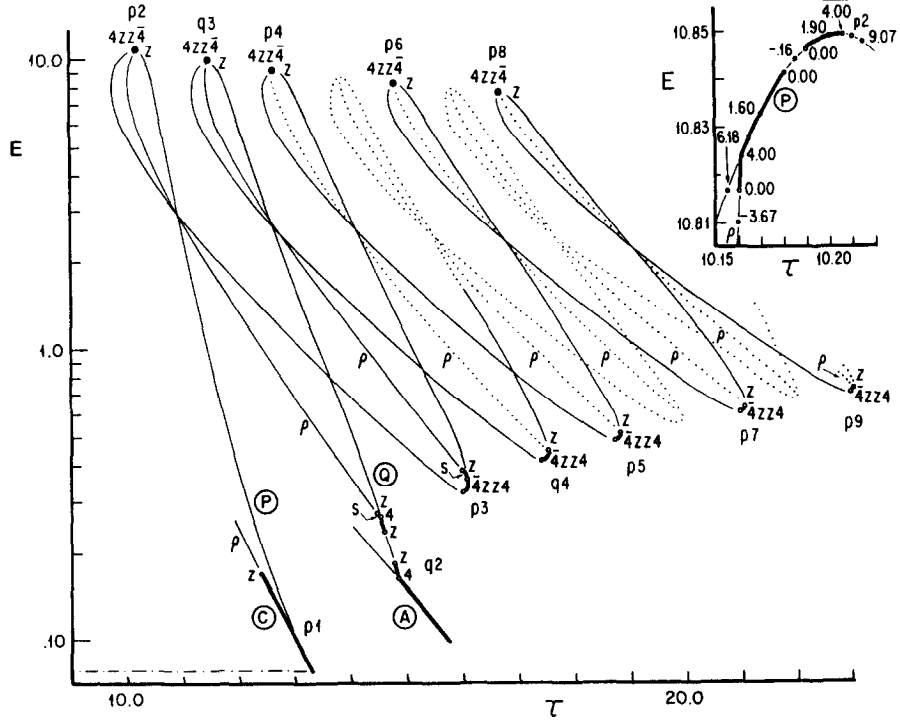

FIG. 3. E–τ plot for a duet of asymmetric librations, P and Q, together with their connecting rotations. As shown in Fig. 2, P begins as a period-tripling from the vertical family while Q is an isochronous branch of the A family. Actually calculated curves are shown as thick or thin solid lines, while the dotted curves are guesses. The points p1, p2, etc. and q1, q2, etc. are points on the P and Q curves, respectively, and are referred to in Fig. 16. Near every sharp turn of P or Q, there are two small stable regions bounded by a $\bar{4}$, two Z's, and a 4 (where the rotation branches). One of these regions, near point p2, is shown in detail in the inset.

An example of a family of periodic trajectories is given in Fig. 1, which shows a few members of the "boomerang" family, or B family, a symmetric libration. We have roughly 4000 such trajectories, comprising roughly 40 families. We have taken special pains to identify all the branchings occurring on the important families and to follow all the new families originating at these branchings. This task is endless, however, and we have concentrated on the simplest families and their isochronous branchings. The number of period-doublings encountered grows very rapidly and the corresponding trajectories become very complicated, so that we soon had to stop following them all. Those which we actually show on our E–τ plots are connected to their parent family by a dot–dashed horizontal line.

III. Numerical Results for the Periodic Trajectories of NELSON

A. *E–τ Plots and Trajectory Shapes for the Most Important Families*

Figure 2 is an E vs τ plot of the main symmetric families. This figure also shows the beginnings of asymmetric branchings, two of which are shown in Fig. 3. Figure 4 is a blowup of a typical small region of stability shown on the E–τ plots.

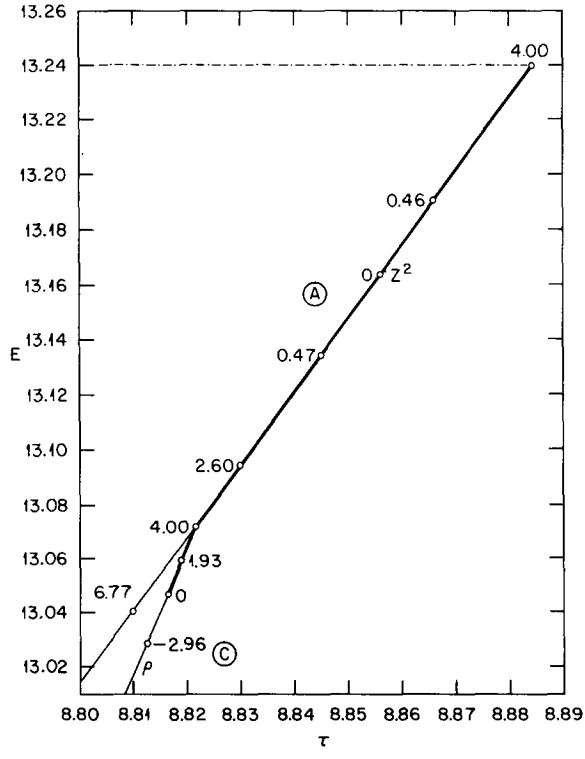

FIG. 4. Detailed blowup of the E–τ plot for the small region in which A branches as a period-doubling from V ($4Z^24$ in Figs. 2 and 5) and C branches isochronously off of A.

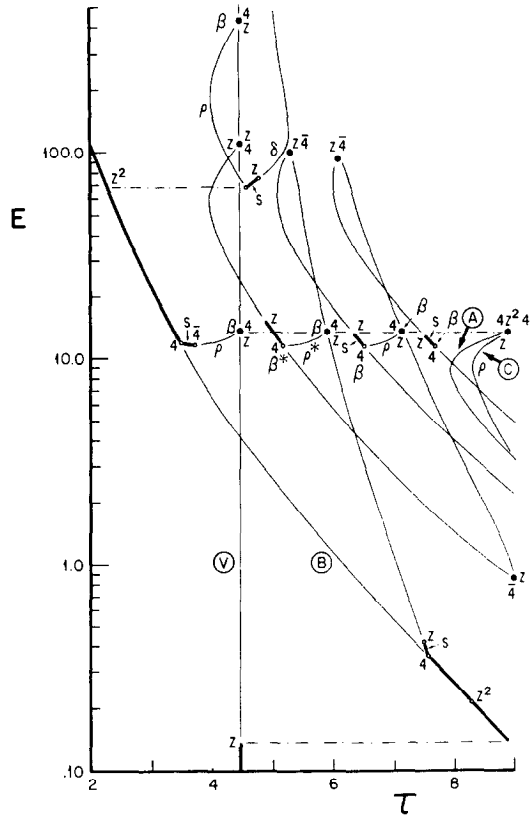

FIG. 5. E–τ plot of the simpler branchings from the V (vertical) and B (boomerang) families. All unnamed librations and their connecting rotations are asymmetric. The symbols β, β^*, δ, and ρ^* are defined in Section III.

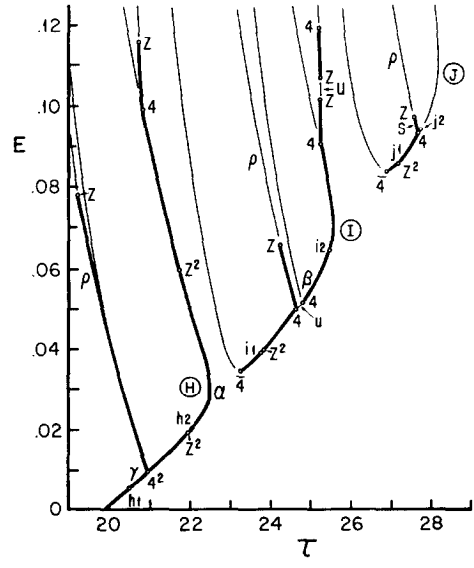

FIG. 6. E–τ plot of the low-energy parts of the symmetric H, I, and J families. The symbols α, β, and γ are defined in Section III. The points h1, h2; i1, i2; and j1, j2 correspond to trajectories of H, I, and J respectively and are referred to in Fig. 15.

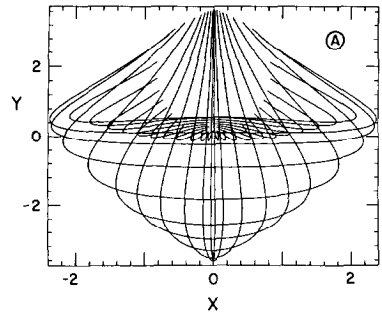

FIG. 7. x–y plot of the entire A family. At low energy this symmetric libration begins as a period-quadrupling of the vertical family, while at high energy it branches onto the same vertical as a period-doubling.

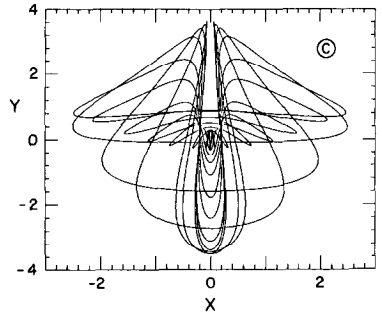

FIG. 8. x–y plot of the entire C family, a symmetric rotation. At high energy this family branches isochronously off the A family, very close to the place where the latter branches off the vertical. (See Fig. 4.) At low energy the C family begins (together with P) as a period-tripling of the vertical.

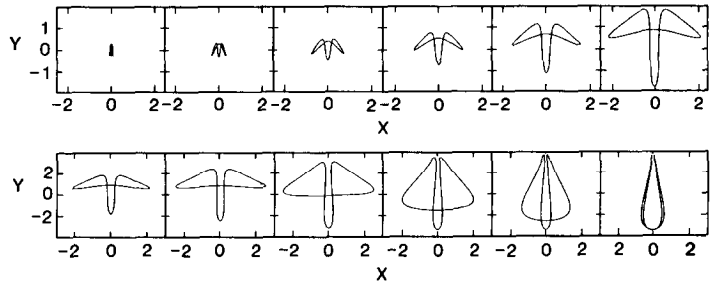

FIG. 9. Sequential x–y pictures of single trajectories for the C family, showing the transition from low to high energy. The x and y scales are different for the top and bottom of frames; the last picture on the top row is the same as the first picture on the bottom row.

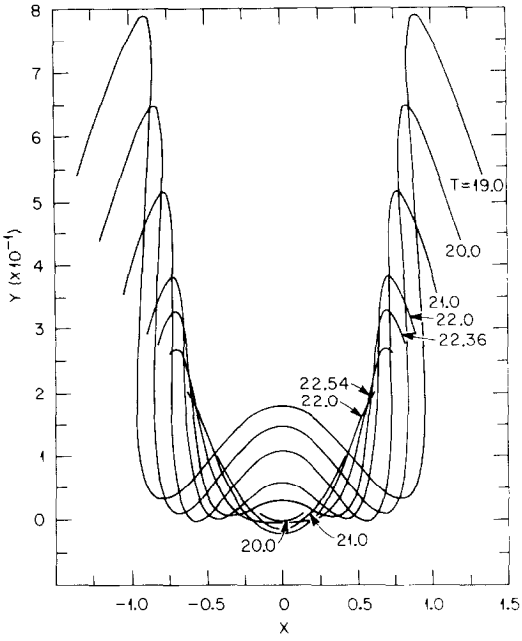

FIG. 10. x–y plot of members of the **H** (or horizontal) family at relatively low energies. This family is a symmetric libration.

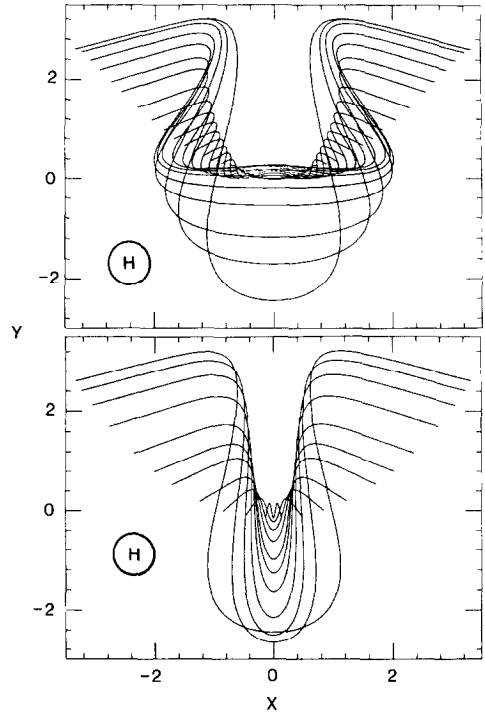

FIG. 11. x–y plots of the entire H family. The upper picture shows the behavior from very low energy to the point at the top of the E–τ curve in Fig. 2. The lower picture shows the transition from the top to a point close to where the H family branches from the vertical as a period-quadrupling.

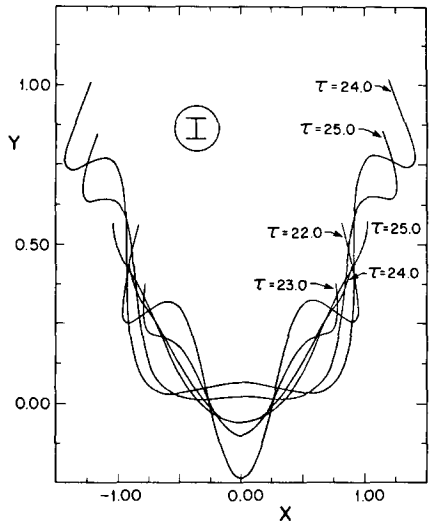

FIG. 12. x–y plot of members of the I family at relatively low energies. This family is a symmetric libration.

Then Fig. 5 is a detailed E–τ plot of the simpler branchings of the V and B families, while Fig. 6 shows the low-energy E–τ plot of the H, I, and J families. The trajectories of the main symmetric families B, A, C, H, I, and J are plotted in Figs. 1 and 7–15. Trajectories for the two asymmetric families P, Q of Fig. 3 are plotted in Fig. 16. The figure captions give many details of the complicated behavior of the various families.

In the low-energy limit, all this complication reduces to two very simple har-

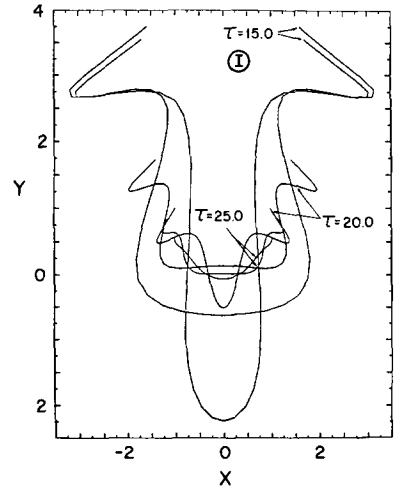

FIG 13. x–y plot of the I family, showing the behavior over the entire cycle in Fig. 2. For each τ there are two different trajectories.

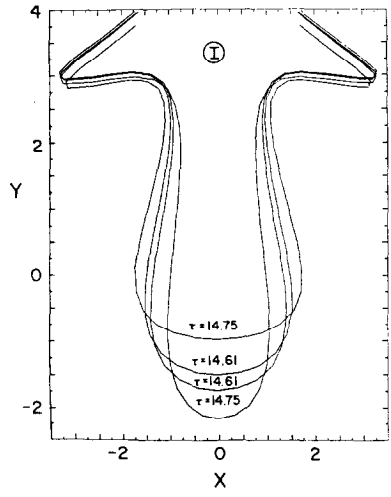

FIG. 14. x–y plot of the detailed behavior of the I family near the top of the cycle in Fig. 2. Note that, in this region, the bottom part of the trajectory is very sensitive to small changes in τ.

monic oscillations, one horizontal, one vertical, with two noncongruent periods. Note, however, from Eq. (5), that $V(x=0, y)$ is purely quadratic and therefore the vertical oscillations (V family) retain their linear harmonic behavior and their constant period for all amplitudes; they appear in the E–τ plots as a vertical line. This is not so for the horizontal oscillations (H family); Figs. 10 and 11 show what happens to them as their amplitude increases. A naive expectation might have been that this family, as it grows, occupies the bottom of the NELSON valley and can be identified with the collective oscillations of nuclear physics. Figure 10 shows that this is true for a while but then, suddenly, the trajectories start leaving the valley to

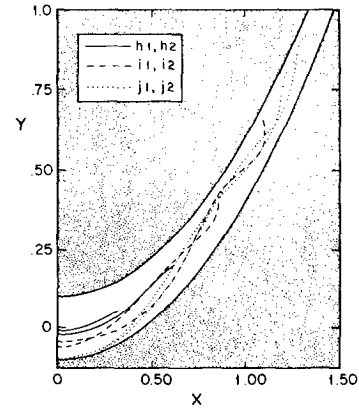

FIG. 15. x–y plot of various H, I, and J trajectories which lie in the valley of the NELSON potential. These trajectories correspond to the points labeled h1, h2; i1, i2; and j1, j2 in Fig. 6. The unshaded region is the valley of the potential, defined by $y = 0.5x^2 \pm 0.1$. These librations are all symmetric about $x=0$; hence, we show only the right-hand part of each.

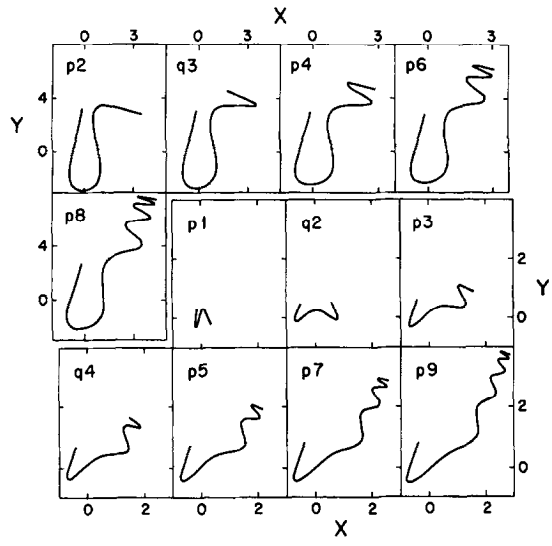

FIG. 16. Sample trajectories for the P and Q families, which are asymmetric librations, taken at the points p1 to p9 and q1 to q3 indicated in Fig. 3. Note that a new "hook" is added on the right of each trajectory with each turn of the screw in Fig. 3.

climb the walls. This corresponds to a sharp left turn in the E–τ plot (symbol α of Figs 2 and 6). Another family, the I family, comes down from the mountains then, occupies the valley for a while, and returns to the mountains (Figs. 2, 6, and 12). Later the J family comes down, stays for a while, and goes back up, etc. The real picture is thus vastly more complicated than that of a single, continuous, collective family. From Figs. 6 and 15, one realizes that the "valley trajectories," instead of

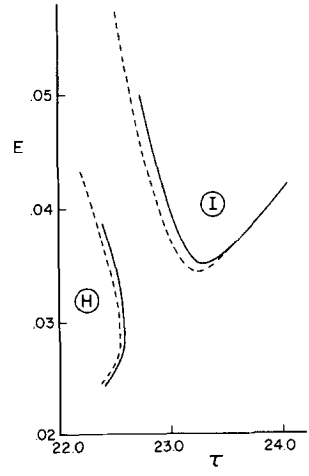

FIG. 17. Behavior of the H and I families near the gap. The dashed curve is for $N = 96$ and the full curve is for $N = 192$, where N is the total number of time-steps as given in Eqs. (2) and (4). Note that on this E–τ plot we do not adhere to the conventions for stable and unstable lines mentioned in Section II.

forming a single continuum, are divided among sections of the H, I, J, and presumably higher families. Also, Figs. 10, 12, and 15 show that a new "hook" is added to both ends of the trajectory shape each time one switches to the next more complicated valley family. Note that in Figs. 2 and 6 there is a sizable gap between the H and the I families, and another between I and J, so that there are values of τ for which no valley trajectory exists. Figure 17 shows that such a gap does not depend on the dimensionality used to perform the numerical calculations [2]. Doubling the size of the space leaves the gap essentially unchanged. These gaps seem to be due to a resonance between the frequency of the valley oscillations and that of the transverse oscillations. A similar resonant gap appears near the top (symbol δ) of Fig. 5, and there are many others.

B. *Examples of Interesting Branchings from the Main Families*

As we can see from Figs. 2 and 5, a number of interesting simple branchings arise from the V and B families. Figure 18 shows four branchings from the B family. If we start at the bottom of the B curve in Figs. 2 and 5, we find the double, open boomerang, a period doubling from the lower Z^2 point; the asymmetric boomerang, an isochronous branching (lower 4); the open boomerang, an

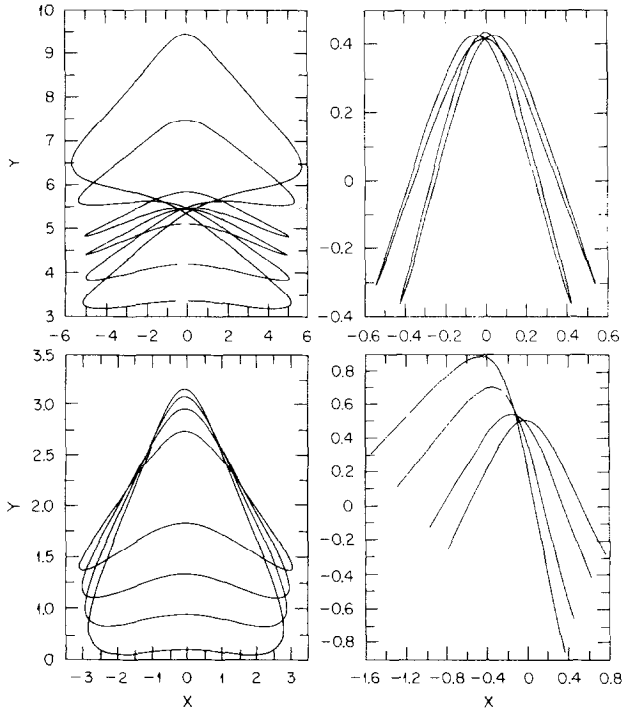

FIG. 18. x–y plots of four branchings from the B family. Clockwise from the top right we have double open boomerang (symmetric rotation), asymmetric boomerang (libration), open boomerang (symmetric rotation), and double mushroom (symmetric rotation).

isochronous branching (upper 4); and the double mushroom, a period-doubling (upper Z^2). Each of the Z^2 points is a double solution, and from each Z^2 an asymmetric libration branches off, as well as the symmetric rotations shown in Fig. 18. Further discussion of this point is given in Ref. [10], where the general classification of all possible branchings is explored. Figures 19a and 19b show x–y pictures of the rotation and libration from the lower Z^2 point, and in Fig. 20 we give a detailed E–τ plot in the neighborhood of this period-doubling. Then, as we see from Fig. 5, both the open boomerang and the mushroom terminate as isochronous branchings of the vertical family. Figure 21 is an x–y plot showing the behavior of the entire open boomerang family.

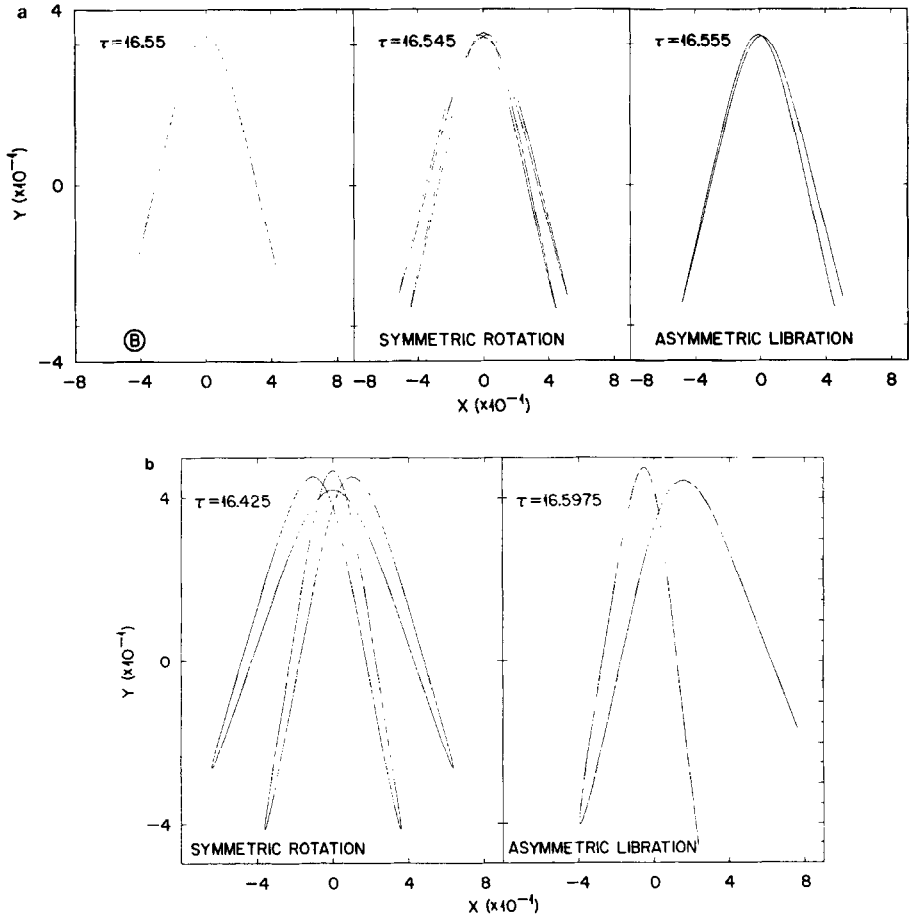

FIG. 19. (a) x–y plots of the symmetric rotation (double open boomerang) and asymmetric libration arising from the period-doubling at the lower Z^2 of the B family. The first picture is the original boomerang and the second and third pictures are the period-doublings, taken close to the branching. (b) Additional x–y plots of the period-doubled families shown in (a). The cases shown are further removed from the branching point than those in (a).

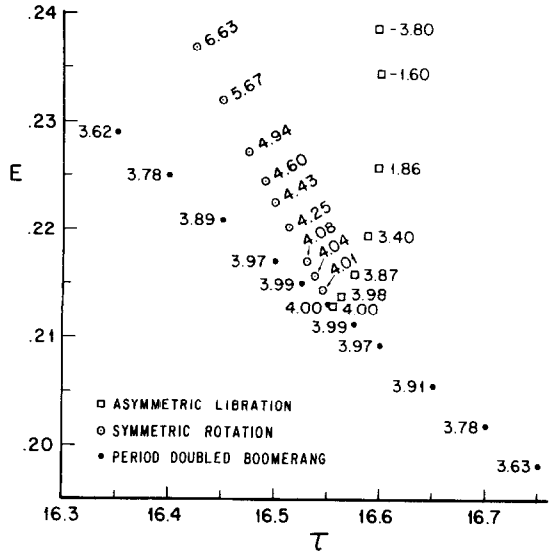

FIG. 20. Detailed E–τ plot of the period-doubling branching at the lower Z^2 of the boomerang family. The numbers give the values of Tr M. Near branching the libration is stable and the rotation is unstable. Note that the rotation and libration converge, with excellent accuracy, to the same point on the period-doubled boomerang curve. Note also that, since the boomerang has Tr $M = 0$ (two eigenvalues $= -1$), the *period-doubled* boomerang has Tr $M = 4$ (four eigenvalues $= +1$).

In general, rotations serve as bridges between librations, thereby giving a mechanism for changing from one librational shape to another. Two examples of asymmetrical rotational bridges are given in Fig. 22 and in Figs. 23 and 24. Also, rotations sometimes connect the *same* libration, an example of which is shown in Fig. 25 for the rotation branching from the top and bottom of the H family.

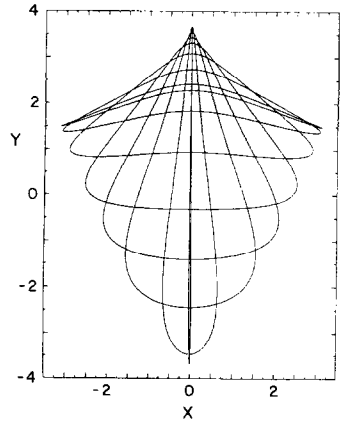

FIG. 21. x–y plot of the entire open boomerang family. This symmetric rotation serves as a simple bridge between the V and B families.

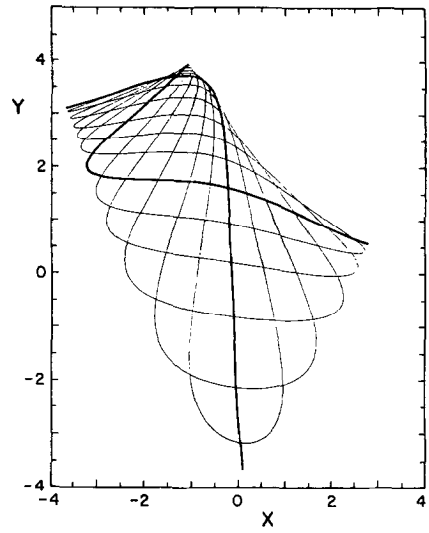

FIG. 22. x–y plot of members of an asymmetric rotation bridge, marked ρ^* in Fig. 5. The heavy lines are the two end librations.

The rotation shown in Fig. 25 begins, at low energy, as a 4^2 isochronous branching from the H family. Therefore, it is part of a double solution (see Ref. [10]) and in Figs. 26a and 26b we show this rotation and its companion libration near branching. Double solutions at branching occur for cases other than Z^2 and 4^2. They also arise from period-multiplying branchings greater than 2. We have never found a double branching from a single period-doubling (Z, *not* Z^2). However, for all period-tripling and period-quadrupling cases studied, there are always two branchings. In Fig. 2 we see that the C and P families arise as a double branching from the period-tripling (Tr $M = 1$) of the vertical family. Similarly, the

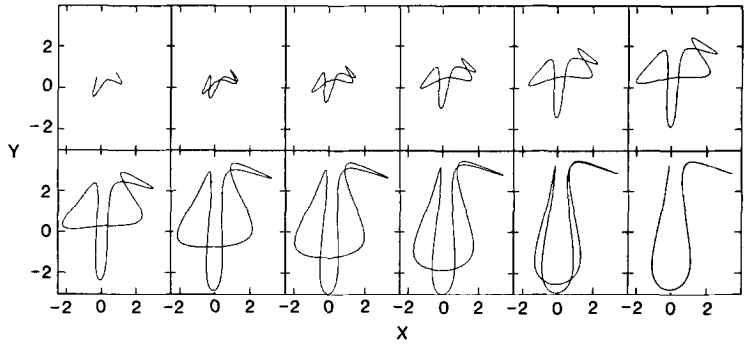

FIG. 23. Sequential x–y pictures of the first rotational bridge shown in Fig. 3. (This is the rotation which begins by branching from Q somewhat above the point q2 and terminates at p2 on P.) The first and last pictures are the branching librations.

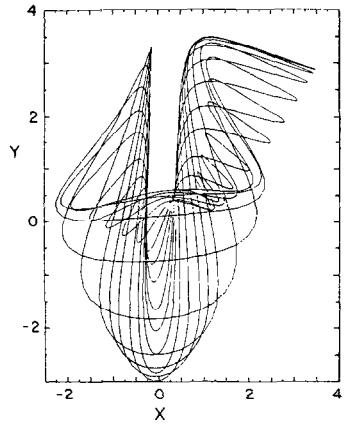

FIG. 24. x–y plot of the entire rotational bridge shown in Fig. 23.

A and H families originate together as a period quadrupling (Tr $M = 2$) from the vertical. In Fig. 27 we present an example of a double branching due to a period-tripling from an asymmetric family; both are librations and both are unstable near branching. However, very close to the branching point both period-tripled trajectories are indistinguishable from the original one and Tr M changes rapidly with τ. Thus, the two curves shown are somewhat removed from the branching region, with values of Tr M which are quite different from their branching value. A detailed E–τ plot of this branching is shown in Fig. 28. Figures 29–32 display the two period-triplings arising from the Tr $M = 1$ points just below and just above the lower Z^2 of the boomerang in Figs. 2 and 5. These two period-triplings look very different, but they are exactly the two cases which are predicted by the analysis of Ref. [10].

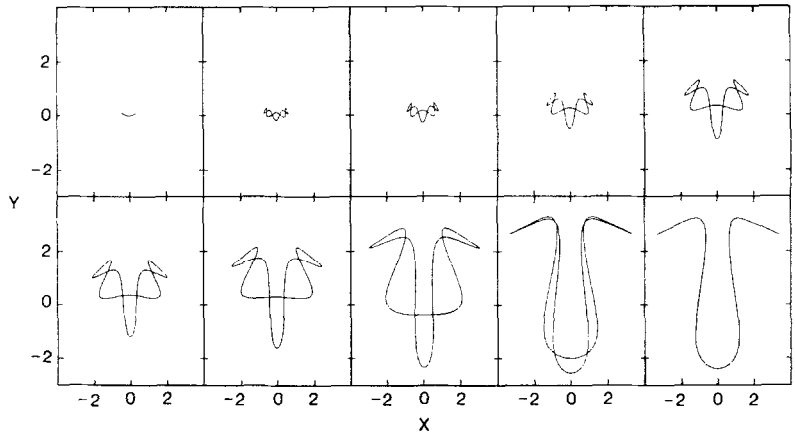

FIG. 25. Sequential x–y pictures of the rotation connecting the top and bottom of the H family (Fig. 2). The first and last pictures are the H family at the branching points.

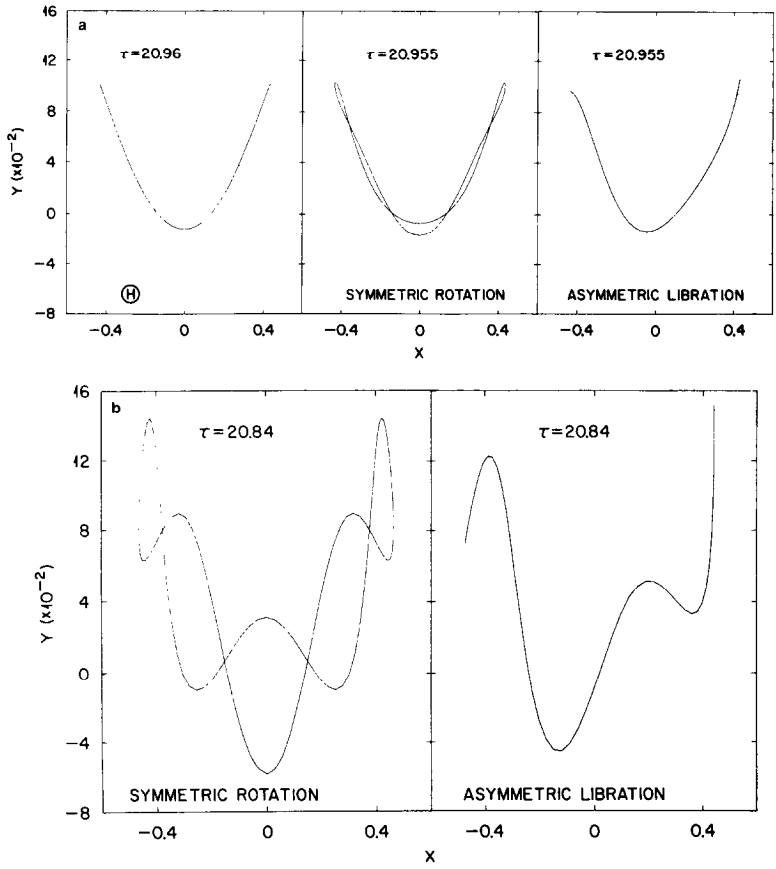

FIG. 26. (a) x–y plots of the symmetric rotation and the asymmetric libration arising from the low-energy 4^2 isochronous branching of the H family (first picture). The second and third pictures are taken close to the branching point, where the rotation is stable and the libration is unstable. (b) Additional x–y plots of the 4^2 branchings shown in (a). The cases shown are somewhat further removed from the branching point than those of (a).

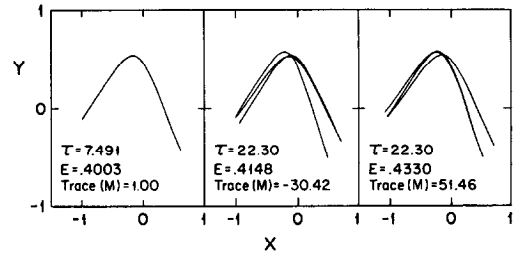

FIG. 27. Period-tripling from the asymmetric boomerang (see Fig. 18). The branching occurs in the small stable region at low energy in Fig. 5, near the point where the asymmetric boomerang branches from B. The first picture is the asymmetric boomerang at the branching point, while the second and third pictures show the continuation of the lower and upper branchings, respectively, shown in Fig. 28.

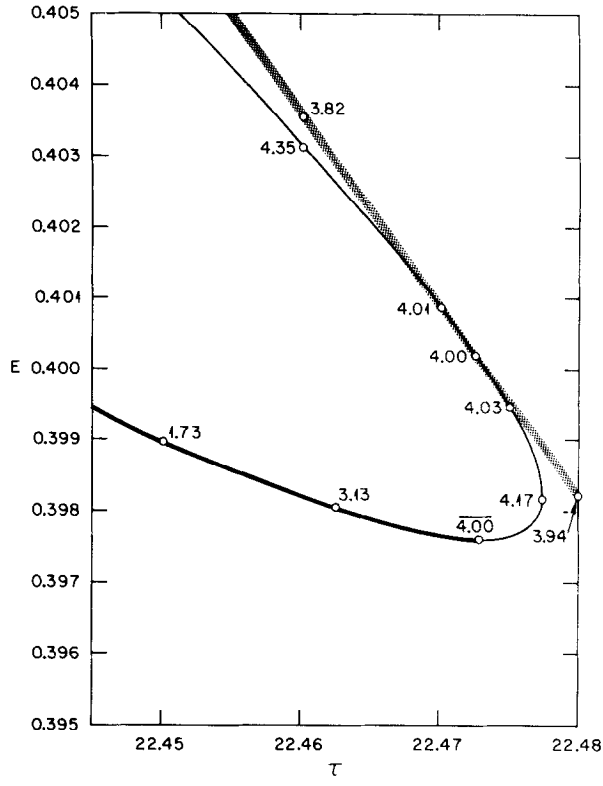

FIG. 28. E–τ plot near the branching of the period-tripling from the asymmetric boomerang. The numbers give the values of Tr M. The shaded curve is the period-tripled asymmetric boomerang. Note that both period-triplings are unstable at the branching point. The picture shows clearly that the Poincaré index (see Section IIID) is conserved as the energy is varied through the branching.

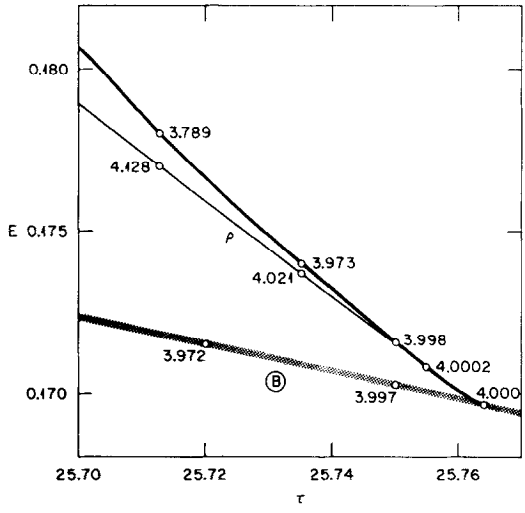

FIG. 29. E–τ plot near the period-tripling from B, for the point at which Tr $M = 1$ just *below* the lower Z^2 point in Figs. 2 and 5. The shaded curve is the period-tripled boomerang. The numbers give the values of Tr M.

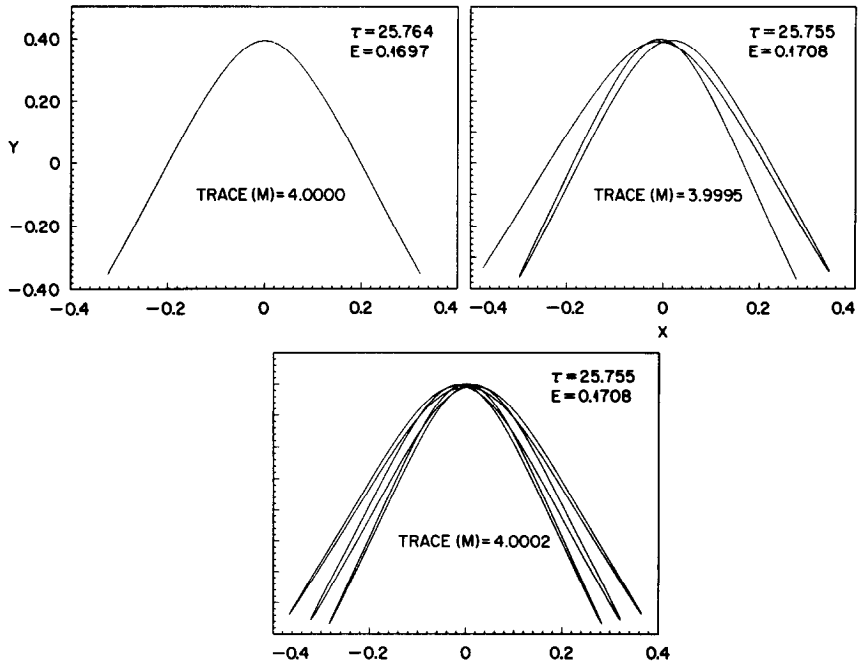

FIG. 30. x–y plots of the period-tripling shown in Fig. 29. The first picture is the boomerang, while the second and third pictures show the branchings. The asymmetric libration is stable and the symmetric rotation is unstable.

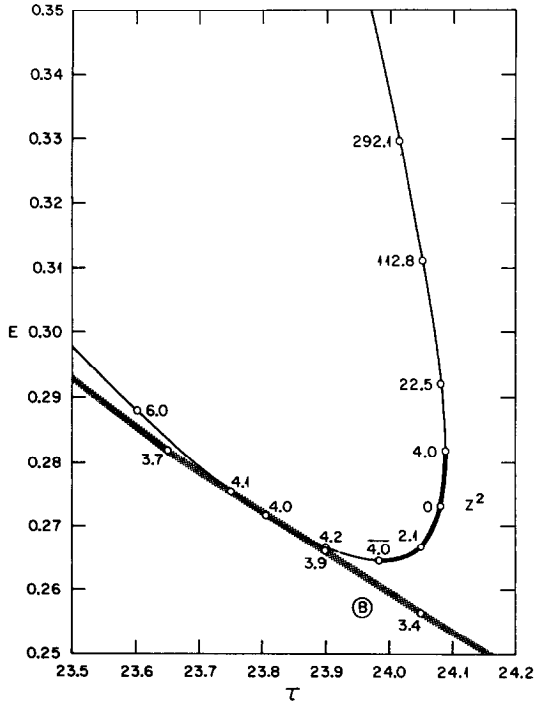

FIG. 31. E–τ plot near the period-tripling from B, for the point at which Tr $M = 1$ just *above* the lower Z^2 point in Figs. 2 and 5. The shaded curve is the period-tripled boomerang. The numbers give the values of Tr M.

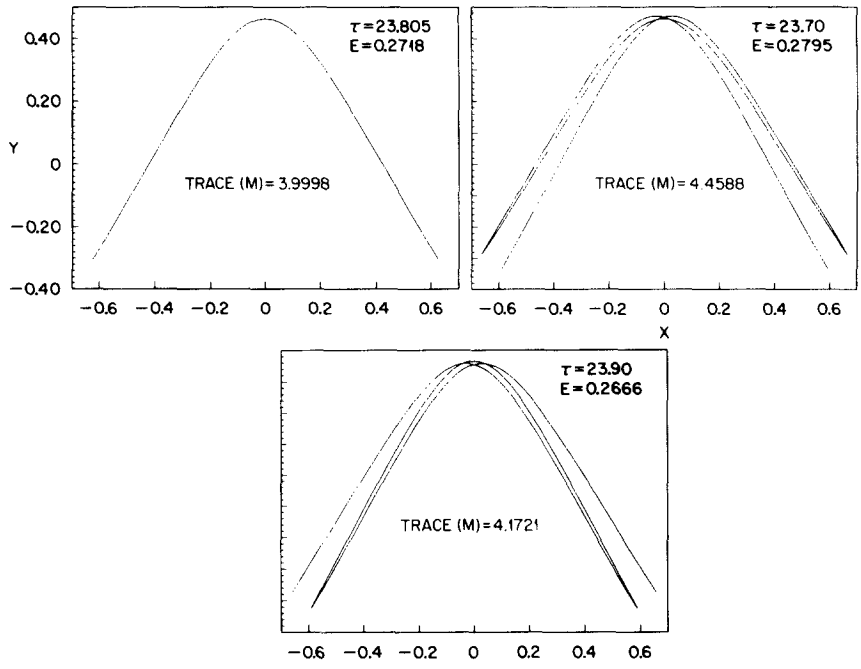

FIG. 32. x–y plots of the period-tripling shown in Fig. 31. The first picture is the boomerang, while the second and third pictures show the branchings. Both symmetric librations are unstable at the branching. However, the libration in the third picture very rapidly goes through a $\bar{4}$, is briefly stable, and then becomes unstable again, as shown in Fig. 31.

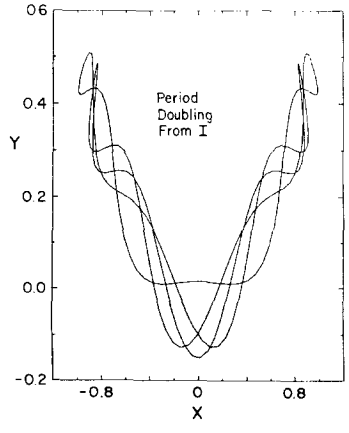

FIG. 33. x–y plot of a trajectory obtained by a period doubling from the Z^2 occuring at low energy for the I family.

In general, period-multiplied trajectories can become exceedingly complicated. Figure 33 shows an example of the x–y plot of a *single* trajectory obtained from a period-doubling of the I family. This trajectory is a symmetric rotation with many loops. Since this branching arises from a Z^2, there is also a companion family which is an asymmetric libration.

C. *Topology of the E–τ Plots*

The continuous line which represents a family on the E–τ plot cannot begin or end, except for one of two reasons: (1) it branches upon another family or (2) it becomes the family of small oscillations about an equilibrium point. Terminations of the second type are easily enumerated: one for the V family and one for H. All other terminations must be of the first type. For instance, the other end of the H family terminates at a period-quadrupling of the vertical oscillations (Figs. 2 and 11). Note that we have never found an isochronous branching (i.e., Tr $M = 4$) for which it was not obvious which family continues through the branching, and which family or families terminate there. Some families do not terminate anywhere; either they go on to infinity in the E–τ plane (the V and B families do this at high energy), or they form closed curves (as do the I and J families).

A related topological question concerns the connectedness of the entire E–τ plot. Figure 2 shows that H and V are connected in several ways, B, C, and A being part of the same cluster. As far as we know, I and J, together with their associated rotations and asymmetric librations, are not connected to this cluster; they constitute two islands. This could still be wrong if a connection existed through the period-multiplied trajectories, which is a problem we have not investigated. If they are islands, however, then it is not possible to generate the entire E–τ plot by the well-defined and systematic procedure which consists of starting at a known point and following all the branches by continuity.

The topoly of the E–τ plot is definitely not that of a tree. The plot has many possible cycles, or closed paths. Figure 2 shows that the H, I, and J families all exhibit such cycles. There are also islands, as we just pointed out. In this regard, the J family (shown in Fig. 2) is particularly striking since the only isochronous branchings from it give rise to the rotation connecting the top and bottom of the island. The only other branchings from J and this rotation are period-doublings and higher-order period-multiplying branchings.

There is an interesting topological difference between the librations and the rotations. The librations are more persistent; a typical librational family has a longer curve in the E–τ plane, with more of a variety of branches attached to it. Thus, it becomes natural to consider the librations as the "more important" families. The rotations, on the other hand, always form rather short bridges between two librations, or sometimes (as in the H, I, and J families; Fig. 2) between two parts of the same libration. An outstanding example of this very general difference is given in Fig. 3, which shows the two asymmetric librations P and Q. Each of these executes a large number of screw-like excursions in the E–τ plane, keeping

out of step with each other. A whole series of rotation bridges connects P and Q every half-turn of the screw. The net effect reminds one of a DNA molecule in two-dimensional projection. Every other asymmetric libration which we have examined in this region of the E–τ plane has turned out to do something similar. An analogous situation prevails for the asymmetric librations of the region covered by Fig. 5, except that the range of energy variation is larger and the short rotation bridges occur at intermediate energies.

D. *Some Empirical Rules*

The analysis of all possible branchings had been done much earlier by Meyer [17] for the generic case, in which the problem possesses no symmetry at all. In particular, Meyer found that isochronous branchings did not exist and that, in all places with $\mathrm{Tr}\, M = 4$, the E–τ curve should have a horizontal tangent, without branching. We have many examples of this behavior; we call such points "horizontal fours," and we designate them on the E–τ plots by $\bar{4}$. It is an important result of our work, however, that isochronous branchings come into existence as soon as one symmetry is present, either $x \to -x$ or time-reversal. Asymmetric rotations, which have no symmetries, are the only families from which no isochronous branchings can occur. Branching 4's are abundant from asymmetric librations and symmetric rotations, both of which have one symmetry, and branching 4^2's show up for symmetric librations, which have two symmetries. At a horizontal 4, the M matrix has a single eigenvector, namely, the vector corresponding to an infinitesimal time-displacement along the trajectory; at a branching 4 it has two distinct eigenvectors, one of which is the time-displacement vector.

A very important fact is that, within a given family, there may be more than one stable region. Indeed, there may be an infinity of such regions. An obvious example is the B family (Figs. 2 and 5) which starts stable at low energy, has some important branchings, becomes unstable until $E = 11.8$, then enjoys another extended region of stability, apparently lasting all the way to infinity. Similarly, the V family has very small recurring regions of stability at higher and higher energies. This fact means that the standard scenario [15] in which the stability is passed on by period-doubling to successively more complicated trajectories, though very attractive in its universality, can miss a lot of the information.

The standard scenario suggests that there might be something like "conservation of stability" at a branching. This is indeed true, but what is meant by it needs to be defined precisely. This is accomplished by means of the "Poincaré index" [16]. To every elliptic periodic point on the Poincaré map, one assigns the index $\sigma = +1$; to every hyperbolic periodic point, one assigns $\sigma = -1$. The total Poincaré index is the sum of all the individual σ's, i.e., $P = \Sigma_i \sigma_i$. This remains conserved as energy is varied through a branching. In other words, the quantity which is conserved is "stability minus instability." In applying this rule, the symmetries of the branching, such as time-reversal or $x \to -x$ symmetry, must be taken into account. The various possible Poincaré maps are shown in Ref. [10]. Here we illustrate only a few cases.

For instance, varying the energy across a "horizontal four," we see an equal number of stable and unstable branches appear or disappear; hence, P is conserved. Consider the point labeled β on the I family in Fig. 6. For energies just below β, we have one unstable trajectory, a symmetric libration; hence $\sigma = -1$ and $P = -1$. For energies just above β, we have one stable symmetric libration with $\sigma = +1$ and *two* unstable asymmetric librations (obtained from each other by $x \to -x$), each with $\sigma = -1$; hence $P = -1$ again. A similar argument holds for all the points labeled β in Figs. 2, 5, and 6. Consider, for instance, the point labeled β^* in Fig. 5. For energies just below β^*, we have one unstable asymmetric libration; hence $P = -1$ (the mirrored asymmetric libration traverses the Poincaré section in a completely different part of the plane and does not need to be considered). For energies just above β^*, we have one stable asymmetric libration with $\sigma = +1$ and *two* unstable asymmetric rotations (obtained from each other by *time-reversal*), each with $\sigma = -1$; hence $P = -1$ again. At the point γ in Fig. 6 (see also Figs. 26a and 26b), the σ contributions from the two unstable asymmetric librations (mirror images of each other) and from the two stable symmetric rotations (time-reverses of each other) cancel, so that P is conserved again. Finally, one can check easily that P is conserved for the period-tripling of the asymmetric boomerang, shown in Figs. 27 and 28, and for the two period-triplings of the boomerang, shown in Figs. 29–32. In general, we found that every calculated branching fitted into the theoretical classification of Ref. [10].

IV. Some Nonperiodic Trajectories of NELSON

We now present a short study of the behavior of the nonperiodic trajectories which lie in phase space close to a periodic trajectory. The NELSON potential is particularly convenient for this since, by energy conservation, all trajectories remain in a finite region of phase space, and therefore they are recurrent [14]. We obtain these trajectories by integrating the equations of motion (2) without imposing the

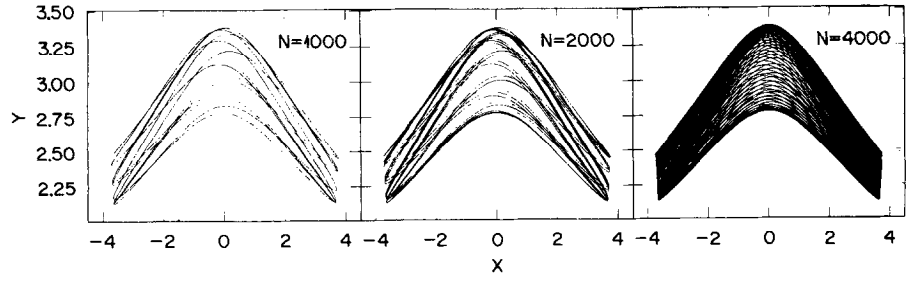

FIG. 34. x–y plots of a nonperiodic trajectory showing the new paths it traverses as we increase N, the total number of time-steps. The parameters used are $x_0 = 0.001$, $y_0 = 3.15$, $x_1 = 0.152$, $y_1 = 3.14$, and $\varepsilon = 0.03125$.

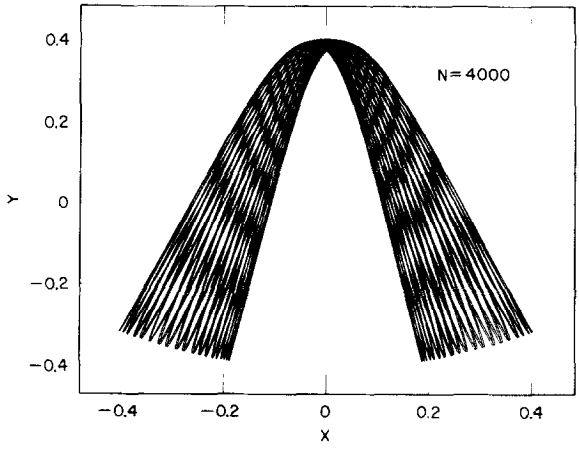

FIG. 35. x–y plot of a nonperiodic trajectory with the parameters $x_0 = 0.02$, $y_0 = 0.39$, $x_1 = 0.011$, $y_1 = 0.40$, $\varepsilon = 0.0912$, and $N = 4000$.

periodicity conditions (3). If the initial conditions (x_0, y_0, x_1, y_1) are close to those which generate a periodic trajectory, we say that the nonperiodic trajectory is "close" to the periodic one.

According to the now well-known KAM analysis [13, 14], the nonperiodic trajectories should be of two kinds. A "regular" trajectory remains confined to a two-dimensional torus in phase space; a "chaotic" one is dense over a finite fraction of the three-dimensional energy shell. We expect those nonperiodic trajectories which are close to a stable periodic trajectory to be regular, and those close to an unstable periodic trajectory to be chaotic. In the following we show examples of both. The

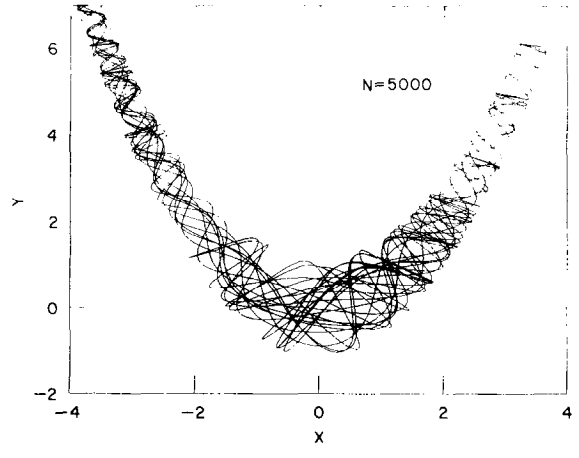

FIG. 36. x–y plot of a nonperiodic trajectory, with the parameters $x_0 = 0.01$, $y_0 = 0.961$, $x_1 = 0.062$, $y_1 = 0.962$, $\varepsilon = 0.0566$, and $N = 5000$.

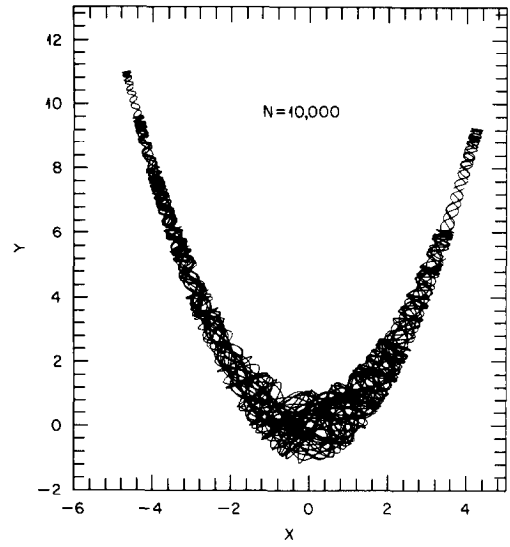

FIG. 37. x–y plot of the case shown in Fig. 36, with $N = 10{,}000$.

parameter ε is taken to be the same as that for the periodic trajectory. The integer N just measures the number of time-steps over which we solve the equations of motion (2).

We have chosen three nonperiodic trajectories lying close to three members of the boomerang family, which exhibits the simplest nontrivial periodicity. Figure 34 gives x–y plots of a trajectory very near a member of the boomerang family in the *upper stable* region shown in Figs. 2 and 5 ($\tau = 3.0$, $E = 21.71$. Tr $M = 1.45$).

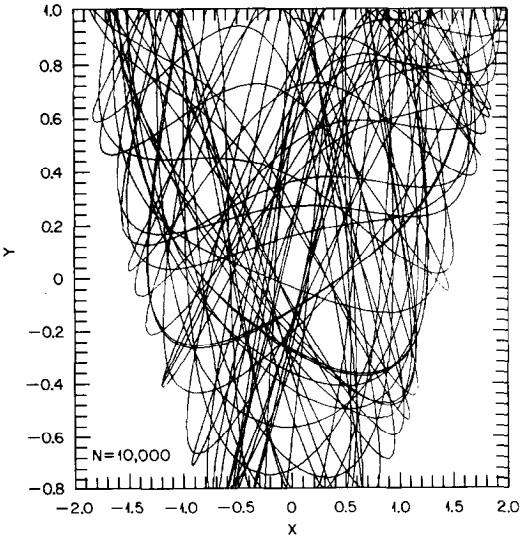

FIG. 38. Blowup of Fig. 37 near the origin.

Figure 35 shows an x–y plot of a nonperiodic trajectory lying near a boomerang trajectory in the *lower stable* region of Figs. 2 and 5 ($\tau = 8.75$, $E = 0.15$, Tr $M = 2.40$). In both Figs. 34 and 35, the nonperiodic trajectory has an envelope shaped like and surrounding the original boomerang trajectory (see Fig. 1). Such trajectories remain on a torus and have also been called quasiperiodic [14].

In contrast, Fig. 36 shows an x–y plot of a nonperiodic trajectory which starts off close to a member of the boomerang family in the *middle unstable* region of Figs. 2 and 5 ($\tau = 5.44$, $E = 1.74$, Tr $M = 17.17$). This trajectory is clearly chaotic. It starts out near the original boomerang but, pretty soon, it leaves it and, instead, wanders, more or less at random, in the valley of the NELSON potential, subject only to conservation of energy. Comparing Figs. 36 and 37, we see the effect of increasing the number of time-steps from 5,000 to 10,000. Figure 38 shows a detailed picture of Fig. 37 near the origin.

Figures 34–38 illustrate an important difference between regular, or quasiperiodic, and chaotic trajectories [14]. Since a regular trajectory remains on a torus, its velocity vector at any particular point of x–y space can have only one of two directions. This gives rise to a "cross-hatched" pattern, which is nicely illustrated in the last frame of Fig. 34 and in Fig. 35. However, the trajectory shown in Figs. 36–38 does not remain on a torus, and, at any x–y point, the velocity vector can be in *any* direction. This fits in with the chaotic aspect of this trajectory.

ACKNOWLEDGMENTS

Early conversations with Marcos Saraceno had a decisive influence on the shaping of this project; had he not shared with us his thinking and exposed us to the multitude of his ideas, this work would never have happened. Much is also due to Emerson J. V. de Passos, from whom we learned many new facts of mordern classical mechanics and semiclassical quantum mechanics. Our other Brazilian friends, Marcus A. M. de Aguiar, Coraci P. Malta, and Alfredo M. Ozorio de Almeida, developed a complete classification of possible branchings with which we were able to check our empirical results. Nelson Rabello, Jr. was involved in the early days and lent his name to the potential. John Negele contributed, as always, with searching questions and comments which we found most stimulating.

Financial support was provided by the U.S. Department of Energy under Contract DE-AC02-76ER03069 with MIT and Contract DE-AC05-84OR21400 with Martin Marietta Energy Systems, Inc., and by the National Science Foundation under Grant INT-8212846.

REFERENCES

1. H. POINCARÉ, "Les Méthodes Nouvelles de la Mécanique Céleste," Vol. I, Chap. III, Art. 36, Gauthier-Villars, Paris, 1892. Translation by M. Baranger.
2. M. BARANGER AND K. T. R. DAVIES, in preparation. For an earlier attempt at calculating periodic trajectories, see Ref. [3].
3. R. H. G. HELLEMAN AND T. BOUNTIS, *in* "Stochastic Behavior in Classical and Quantum Hamiltonian Systems" (G. Casati and J. Ford, Eds.), p. 353, Springer-Verlag, New York, 1979.
4. M. C. GUTZWILLER, *J. Math. Phys.* **11** (1970) 1791; *J. Math. Phys.* **12** (1971) 343; *Phys. Rev. Lett.* **45** (1980) 150; R. BALIAN AND C. BLOCH, *Ann. Phys. (N.Y.)* **69** (1972) 76; M. V. BERRY, *in* "Chaotic

Behavior of Deterministic Systems—Les Houches 1981" (G. Iooss, R. H. G. Helleman, and R. Stora, Eds.), North-Holland, Amsterdam, 1983; E. J. HELLER, *Phys. Rev. Lett.* **53** (1984) 1515; E. J. HELLER, *in* "Quantum Chaos and Statistical Nuclear Physics" (T. H. Seligman and H. Nishioka, Eds.), Lecture Notes in Physics No. 263, Springer-Verlag, New York, 1986.

5. P. BONCHE, S. E. KOONIN, AND J. W. NEGELE, *Phys. Rev. C* **13** (1976) 1226; K.-K. KAN, J. J. GRIFFIN, P. C. LICHTNER, AND M. DWORZECKA, *Nucl. Phys. A* **332** (1979) 109; J. W. NEGELE, *Rev. Mod. Phys.* **54** (1982) 913; R. D. WILLIAMS AND S. E. KOONIN, *Nucl. Phys. A* **391** (1982) 72; M. R. STRAYER *et al.*, *Phys. Letts.* **135B** (1984) 261; K. T. R. DAVIES, K. R. S. DEVI, S. E. KOONIN, AND M. R. STRAYER, *in* "Treatise on Heavy-Ion Science," (D. A. Bromley, Ed.), Vol. III, p.3, Plenum, New York, 1985; A. S. UMAR *et al.*, *Phys. Rev. C* **32** (1985) 172; M. R. STRAYER, *in* "Lecture Notes in Physics," (S. G. Steadman, Ed.), Vol. 219, Springer-Verlag, New York, 1985; PH. CHOMAZ, H. FLOCARD, AND D. VAUTHERIN, *Phys. Rev. Letts.* **56** (1986) 1787.
6. R. DASHEN, B. HASSLACHER, AND A. NEVEU, *Phys. Rev. D* **10** (1974) 4114; S. LEVIT, J. W. NEGELE, AND Z. PALTIEL, *Phys. Rev. C* **21** (1980) 1603; H. REINHARDT, *Nucl. Phys. A* **346** (1980) 1; I. ZAHED AND M. BARANGER, *Phys. Rev. C* **29** (1984), 1010; N. DE LEON AND E. J. HELLER, *J. Chem. Phys.* **81** (1984) 557.
7. M. BARANGER, K. T. R. DAVIES, M. A. M. DE AGUIAR, C. P. MALTA, AND E. J. V. DE PASSOS, *Z. Phys. A* **325** (1986) 491.
8. V. I. ARNOLD, "Mathematical Methods of Classical Mechanics," p. 389, Springer-Verlag, New York, 1978.
9. V. A. YAKUBOVICH AND V. M. STARZHINSKII, "Linear Differential Equations with Periodic Coefficients," especially Chaps. II and III, Keter Publishing House, Jerusalem, 1975.
10. M. A. M. DE AGUIAR, C. P. MALTA, M. BARANGER, AND K. T. R. DAVIES, submitted.
11. M. C. GUTZWILLER, *J. Math. Phys.* **18** (1977) 806.
12. YA. G. SINAI, *Russ. Math. Surv.* **25** (1970) 137; L. A. BUNIMOVICH, *Funct. Anal. Appl.* **8** (1974) 254.
13. V. I. ARNOLD AND A. AVEZ, "Ergodic Problems of Classical Mechanics," Appendix 34, Benjamin, New York, 1968; V. I. ARNOLD, "Mathematical Methods of Classical Mechanics," Appendix 8, Springer-Verlag, New York, 1978; M. V. BERRY, *in* "Topics in Nonlinear Dynamics" (S. Jorna, Ed.), American Institute of Physics, New York, 1978.
14. M. HÉNON, *in* "Chaotic Behavior of Deterministic Systems—Les Houches 1981" (G. Iooss, R. H. G. Helleman, and R. Stora, Eds.), p. 107, North-Holland, Amsterdam, 1983.
15. P. COLLET, J. P. ECKMANN, AND H. KOCH, *Physica D* **3** (1981) 457; J. M. GREENE, R. S. MACKAY, F. VIVALDI, AND M. J. FEIGENBAUM, *Physica D* **3** (1981) 468. The authors of these papers are well aware that the period-doubling scenario does not tell the entire story; see, for instance, J. P. Eckmann, *in* "Chaotic Behavior of Deterministic Systems—Les Houches, 1981," referred to in [4, 14], p. 508.
16. J. M. GREENE, R. S. MACKAY, F. VIVALDI, AND M. J. FEIGENBAUM, *Physica D* **3** (1981) 468.
17. K. R. MEYER, *Trans. Amer. Math. Soc.* **149** (1970) 95.